Journal of the Virtual Explorer, 2004
Volume 15
Paper 1
http://virtualexplorer.com.au/

Fracturing in Polycrystalline Materials

Daniel Köhn

Institut fuer Geowissenschaften, Tectonophysics, University of Mainz, Germany
http://www.uni-mainz.de/~koehn/, *Email: koehn@mail.uni-mainz.de* .

J. Arnold

http://www.uni-mainz.de/~arnold/, *Email: Jochen.Arnold@uni-mainz.de* .

Keywords: Fractures, Elasticity, Discrete, Element Code, Polycrystalline Rocks

Journal of the Virtual Explorer, 2004
Volume 15
Paper 1

Abstract: We present a numerical model for the formation of fractures in rocks at grain scale. The model is based on a discrete approach using a spring network in combination with the "Elle" platform for the simulation of microstructures. In the model grains are defined by clusters of particles that are themselves connected by linear elastic springs that can break. In order to test the model we performed simulations of extension and shortening of a single layer, pure shear deformation of an aggregate with a statistical distribution of grains and studied fracture networks around expanding grains. We investigated the dynamics of fracture propagation, the geometry of fracture patterns and stress distributions as well as the rheological behavior of different materials. The model produces patterns found in natural systems and shows dynamics and behavior of fractures that is in agreement with theoretical models. This type of numerical model offers therefore a useful tool to study specific problems concerning fracture development in polycrystalline rocks.

Table of Contents

Introduction

Brittle deformation of rocks is a very important deformation mechanism in the upper crust of the Earth and at deeper levels if strain rates are high or fluids are involved [Ranalli 1995; Scholz 2002]. Rocks can only sustain very small amounts of strain in the linear elastic regime and fail afterwards [Means 1976]. Failure takes place by the development and propagation of fractures [Jaeger and Cook 1979]. If failure localizes in planar zones, cataclasites will develop in which cohesion of material along grain boundaries is lost and grain size is reduced by intragranular fractures [Price and Cosgrove 1990].

Fractures are generally classified into extensional fractures (Mode I fractures) and shear fractures (Mode II fractures) [Price and Cosgrove 1990; Pollard and Segall 1987]. Mode I fractures develop parallel to the compressive stress and perpendicular to the tensile stress. Since they are oriented perpendicular to the tensile stress they are opening and can be filled with vein material. Mode II fractures are oriented at an angle of less than 45° to the compressive stress. Sliding takes place along these surfaces but they are not opening so that they seldom contain vein material. A combination of mode I and mode II fractures, so termed hybrid shear fractures [Price and Cosgrove 1990] with a smaller angle to the compressive stress than shear fractures show shear displacement plus opening. Which type of fracture develops depends on the stress field and the microstructure of the specimen [Jaeger and Cook 1979]. During progressive deformation different types of fractures may develop successively [Toussaint and Pride 2002].

In addition to their orientation, shape and spacing of fractures is of general interest. These parameters may give insight into the rheology of fractured material and the degree of deformation it has experienced [Price and Cosgrove 1990]. The distribution of fractures, their shape, spacing and formation of three-dimensional networks are also important in the understanding of fluid flow, waste dispersal and the characterization and modelling of oil reservoirs.

Fracture dynamics is a complex phenomenon since the propagation of fractures can be highly non-linear. Griffith (1920) already ascribed the low strength of material under tension to stress concentrations at tips of micro-cracks that pre-exist in most materials. Once a micro-crack propagates stress concentrations at its tips will increase which eventually leads to large-scale failure of the material. Under compression the material behaviour is more complex [Mogi 1962]. The link between microscopic and macroscopic behaviour may not be simple under these conditions [Lockner 1998; Okui and Horii 1997; Hazzard et al. 2000] and transitions between different failure types probably exist [Toussaint and Pride, 2002]. Crack tips may also become unstable under certain conditions and show branching [Marder 1993].

Several models have been proposed to simulate fracture-development in two-dimensional systems on different scales (e.g. Hazzard et al. 2000; D'Adetta et al. 2001; Mühlhaus et al. 2001 and references therein). Molecular dynamic models are concerned with fractures at atomic scale whereas models in statistical physics and disordered systems investigate macroscopic behaviour. The latter type of model use simple elements that are representing clusters of grains and have average properties. We present another type of model where we use elements that are smaller than the grain scale so that clusters of elements represent single grains. This allows us to model fracture dynamics on a macroscopic scale that includes the effects of the underlying microstructure.

Model Approach

We developed a two-dimensional discrete element code ("Mike") based on the work of Malthe-Sørenssen et al. (1998) and combined this model with the simulation environment "Elle" [Bons 2000; Jessell et al. 2001, 2003; Piazolo et al. 2001,2002]. The combination of both models allows us to investigate elastic-brittle behavior of complex polycrystalline or layered microstructures. Therefore we can study the influence of microstructural properties on the macroscopic brittle behavior of rocks.

In the discrete element code rigid circular discs or particles are connected with linear elastic springs. Particles are arranged in a triangular lattice so that each particle has a maximum of six neighbors (Figure 1). Such a configuration reproduces macroscopic linear elastic behavior [Flekkoy et al. 2002]. The force acting on a single particle from a connected spring is proportional to the actual length of that spring minus its equilibrium length multiplied by a spring constant. Compressive stresses in the model are thus negative. A particle is in equilibrium when the forces acting on the particle center from different directions cancel out so that the particle has no momentum and will not tend to move. Springs have a predefined breaking threshold that is defined as a critical tensile stress. Once this tensile stress is reached a spring breaks and is removed from the model. The two affected particles that were connected by the

spring still have a repulsive force between each other but lack attractive forces.

Figure 1. Six Neighbours

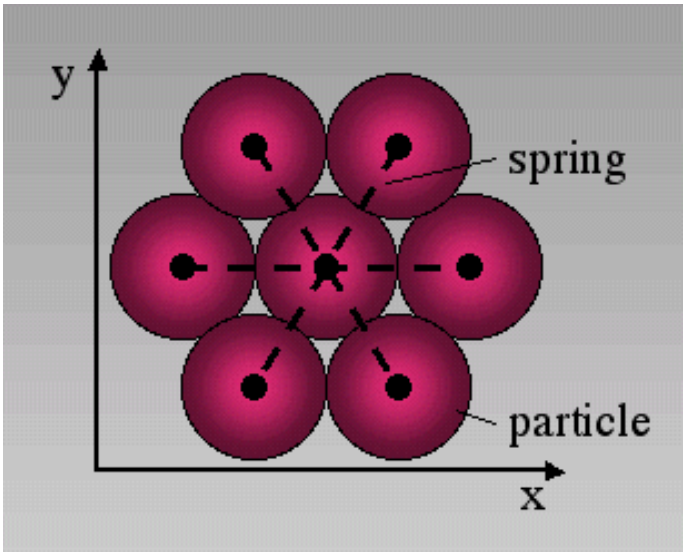

In the discrete element code we use a triangular lattice where each particle is surrounded by six neighbours. Particles are connected by linear elastic springs.

The two dimensional model has the geometry of an initially square area termed the deformation box. Rows of particles on the left and right hand side as well as at the top and bottom of the deformation box are defined as wall-particles (Figure 2). Sidewall and bottom wall-particles are fixed in space perpendicular to the boundary of the box. In order to deform the box wall-particles are moved inwards or outwards to apply compression or extension. Since wall-particles can move parallel to the walls the boundaries do not apply friction. Each time a boundary is moved or a spring breaks in the model a new equilibrium configuration for the lattice is calculated. This is done by a standard over-relaxation method [Allen 1954, Shaw 1953] as described briefly below. In the model each time a wall is moved and the lattice is strained each particle is moved assuming homogeneous deformation. This will remove strain gradients that may result from boundary effects and speeds up the relaxation. Once homogeneous strain is applied the relaxation starts to find a new mechanical equilibrium within the network. Forces on single particles are calculated and particles are moved relative to the resulting force towards their new equilibrium position. In order to attain a more effective relaxation of the whole lattice it is over-relaxed, which means that particles are moved an over-relaxation factor beyond their equilibrium position. This procedure is repeated until a lower threshold is reached that defines the equilibrium of the lattice where particles are stationary. After the lattice reaches force equilibrium the model checks whether or not a spring has reached its critical tensile stress. If this is the case the spring with the highest probability to break will do so and a full relaxation cycle starts again. This procedure is repeated until no more springs break and a new deformation step can start (Figure 3).

Figure 2. Deformation box

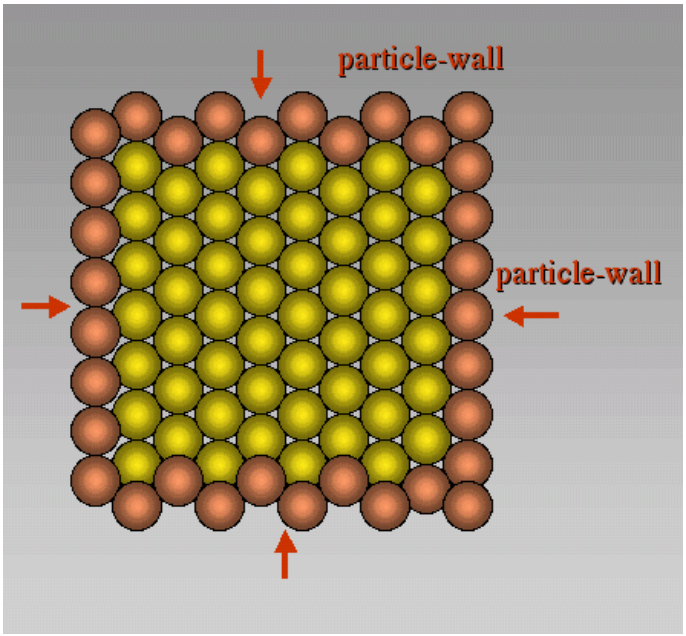

The boundaries or the deformation box are defined by wall-particles. These are shown in brown colour in the figure. Wall-particles are moved in order to strain particles in the box. Wall particles can move parallel to the wall but are fixed perpendicular to it (free slip boundaries). Therefore the walls are frictionless.

Figure 3. Flow of the Program

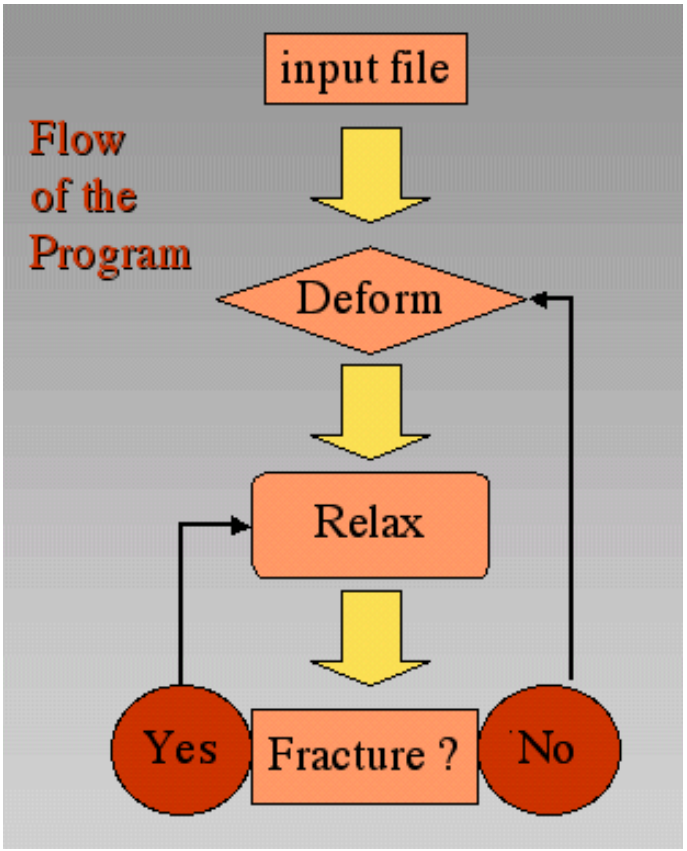

Flow of the Program. First a deformation step is applied on the input structure. After the deformation a relaxation starts in order to find a new equilibrium lattice geometry. Once force equilibrium is reached the program checks if a spring exceeds its tensile strength. If this is the case, the spring with the highest probability to fracture will break and the system is relaxed again. The loop will operate until no more springs fracture. Then the next deformation step is started.

In the "Elle" environment, grains are defined by grain-boundary nodes that are connected by linear elements. In order to combine the "Elle" data-structure with the network of particles in the discrete model the discrete particles present a second layer on top of the "Elle" layer (Figure 4). Particles that lie within an "Elle" grain polygon are defined to be part of that grain. Springs that connect particles of one particular grain will have specific elastic constants and breaking thresholds. Springs connecting two particles of neighbouring grains will have the average spring constant of the two grains and a breaking strength that is characteristic for grain boundaries. In all the presented simulations the grain boundaries are assumed to have a breaking strength that is on average half of the intragranular breaking strength.

Figure 4. "Elle" data structure

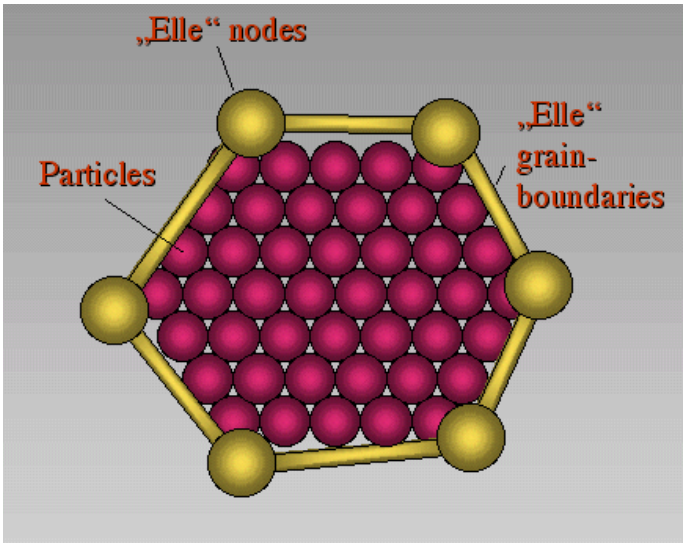

Coupling between the discrete element code and the "Elle" data structure. Elle nodes and connections between these nodes define polygons that may represent grains. Particles that lie within such a polygon are defined to be part of that grain and have the same properties.

Disorder in the system is induced by randomly selecting elastic constants from a Gauss distribution for each grain and randomly selecting breaking thresholds of springs from a linear distribution. Anisotropies in the model can be set by defining layers with different elastic properties. In the presented simulations models consist of 184800 particles for medium resolution and 737600 particles for high resolution. First we will show the development of fractures in a competent layer embedded in a weaker matrix under pure layer parallel extension and compression. Then we will show the development of fractures in polycrystalline materials under pure shear conditions and finally we will discuss fracture patterns around grains that increase in volume. In all simulations we apply a constant strain rate.

Numerical Experiments

Parameters in the simulations are scaled as follows: Strain is dimensionless, the height and width of the deformation box is initially 1.0, and the Poisson ratio of the triangular lattice is 0.33. The elastic constant of springs is by default 1.0. Stresses and tensile strength of springs are scaled with the elastic constant. The tensile strength of springs is by default 0.006. Grain boundary springs are weaker with respect to the default value and distributions of breaking strengths are set around the default value. In

most presented simulations only the elastic constant is varied. This will produce higher or lower stresses in the model at the same strain and will thus induce fracturing at lower or higher amounts of strain. In order to relate model-parameters with real-rock values the elastic constant can be scaled, which then automatically gives real values for stress and tensile strength. Scaling-examples are given in the following paragraphs.

Fracturing of layered material under extension and compression

We performed two simulations with a competent layer that is embedded in a weaker matrix. The initial microstructure is presented in Figure 5a . The smaller grains in the centre make up the vertical competent layer. A resolution of 184800 particles is used (400x462). The elastic constant of grains in the competent layer (non-dimensional value of 1.0) is 100 times larger than that of matrix grains. The tensile strength of all grain-boundary springs is half the tensile strength of intragranular springs and has a non-dimensional value of 0.003. For this simulation the numerical parameters can be scaled to real rock values as follows. If we assume that the elastic constant of grains in the competent layer is 10 GPa (for example) then the breaking strength of grain boundary springs is 30 MPa and grains in the matrix have an elastic constant of 0.1 GPa.

Figure 5. Initial microstructures

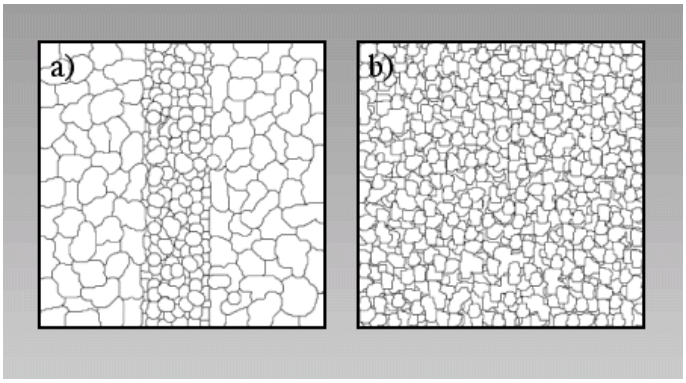

Two different initial microstructures used in the simulations. See text for further explanation.

In the first simulation the layer is extended uniaxial with incremental steps of 0.0025 percent strain (Animation 1). Colours in the animation represent differential stress where blue colours indicate low (0.0) and red colours high (0.003 times elastic constant) differential stresses (Figure 6). In the simulation the stress within the more competent layer rises because it has a larger elastic constant than the matrix. After a while a horizontal stress gradient develops within the vertical layer. Differential stresses are higher at the interface between the competent layer and the matrix than in the centre of the layer. This is an effect of the matrix-layer contact where horizontal stresses are almost zero because of the weak matrix. Geometrical irregularities at the interface of the competent layer to the matrix concentrate stresses where the competent layer is thinner. Once these stress concentrations reach the tensile strength of the springs three fractures develop almost simultaneously and break the whole layer. They show a characteristic spacing, which is found in many natural examples of fractures or joints [Price and Cosgrove 1990]. The fractures develop simultaneously in the model because the tensile strength is reached at the same time at a number of localities along the interface. Once a small fracture forms it will have even higher stress concentrations at its advancing tip because stress scales with the length of the fracture and its tip curvature [Griffith 1920; Jaeger and Cook 1979]. Therefore the fracture will cross the whole layer instantaneously because stress concentrations at its tip are beyond the tensile strength of springs and even increase during propagation (Figure 7). Fracturing will reduce the tensile stress in the competent layer and strain is localized within the fracture while it is opening. The affected area of stress release due to fracturing in the competent layer has a characteristic length-scale, which produces the regular spacing of fractures in the layer. A fourth fracture propagates across the layer shortly after the development of the three initial fractures.

Figure 1. Stiff vertical layer embedded in a weaker matrix

Stiff vertical layer embedded in a weaker matrix under layer parallel extension. Colours show differential stress where red is high and blue low stress. Mode I fractures develop in the layer and show a characteristic spacing. See main text for further explanation.

Figure 6. Stress scale for the simulations

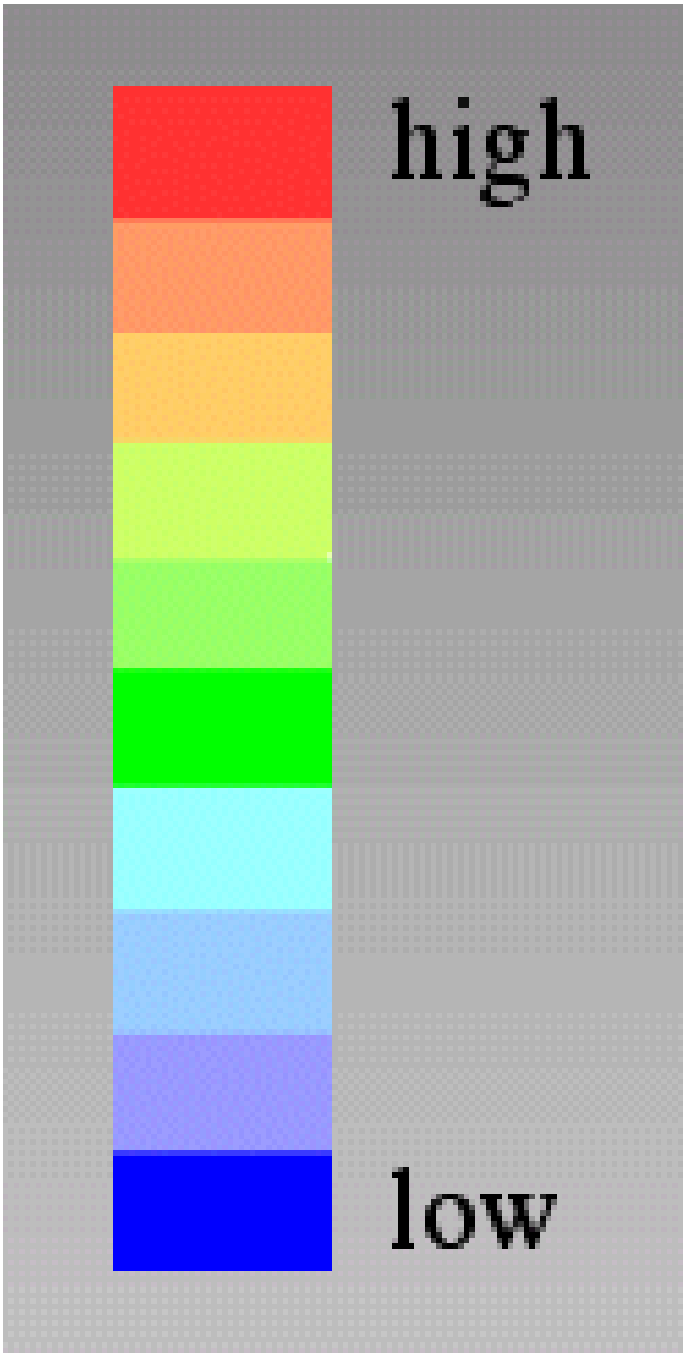

Stress scale for the simulations. Red is high differential stress and blue low differential stress. If the pressure is shown in the simulations then blue colours indicate high and red colours indicate low pressure (horizontal normal stress plus vertical normal stress components).

Figure 7. Differential stress concentrations

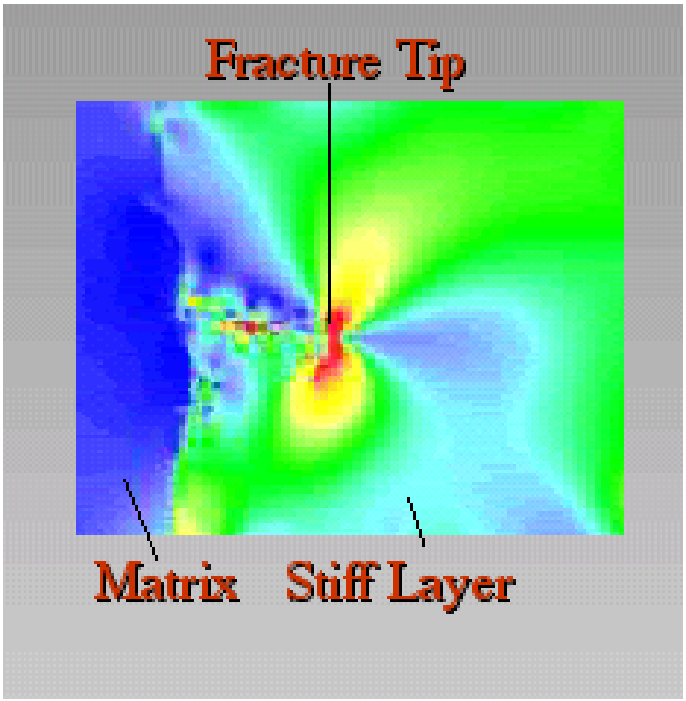

Differential stress concentrations at the tip of a fracture. The layer is extended vertically. The blue colour on the left hand side represents the weaker matrix. The fracture grows from the matrix into the stiff layer. Stress concentrations at the fracture tip drive the propagation of the fracture through the stiff layer.

The stress distribution between two neighbouring fractures has a characteristic geometry (Figure 8). Differential stresses are highest at the interface to the matrix and low in the middle of the layer and next to the existing fractures. New fractures will therefore tend to develop at the interface to the matrix and in the middle between two existing fractures. This happens towards the end of the simulation where a new fracture develops and crosses the layer so that the spacing between fractures is reduced with increasing strain. Once this secondary fracture initiates at the interface to the matrix it can propagate across the layer due to stress concentrations at its tip even if the stress in the centre of the competent layer is not tensile. In addition to the development of new fractures that reduce the spacing the four initial fractures localize strain while they open. However, opening does only effectively reduce stress if the fractures are straight. Since the initial fractures propagate mainly along grain-boundaries they show some curvature and braided geometries. These geometries hinder opening so that additional small-scale fracturing around the existing fractures is necessary in order to accommodate strain. This

successive fracturing results in fluctuations of the stress in the layer throughout the animation. Once the bulk stress in the competent layer reaches the tensile strength of springs (red colour) new small-scale fractures develop and release the stress suddenly or a large fracture develops between existing fractures and reduces fracture spacing.

Figure 8. Stress distribution

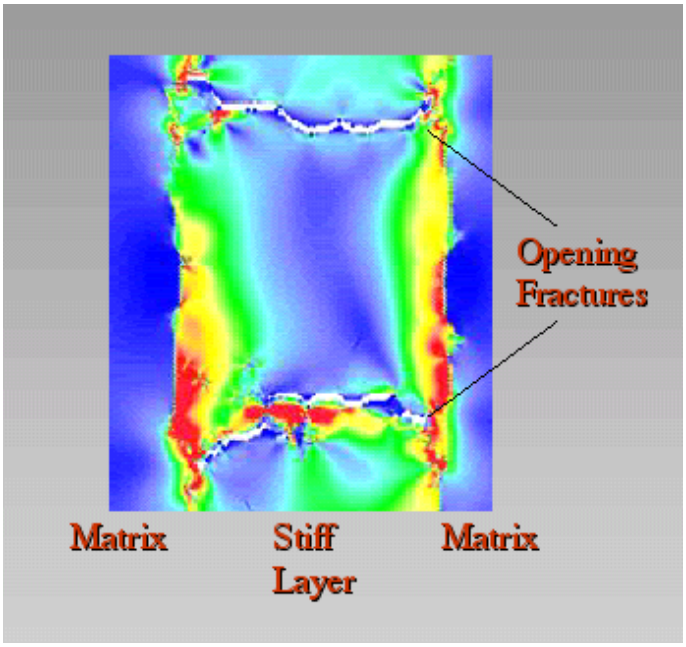

Stress distribution between two fractures in a stiff layer. Extension is vertical. The fractures are localizing strain and are opening. Differential stress is high at the interface to the matrix but low in the centre of the stiff layer. Therefore successive fractures will tend to initiate at the interface of the stiff layer to the matrix.

The second simulation shows a uniaxial compression of the same layer (Animation 2) with a strain of 0.06 percent per deformation step. The colours represent differential stress where blue indicates low (0.0) and red high (0.01 times elastic constant) differential stresses (Figure 6). The strength of the layer under compression is 3.3 times higher than its tensile strength. The initial stress pattern is similar in extension and compression with high differential stresses at the interface to the matrix and stress concentrations at irregularities. While these stress concentrations grow, small mode I tensile fractures develop in regions with highest differential stresses (Figure 9). These fractures are oriented with their long axis parallel to the maximum compressive stress. The behaviour of these mode I fractures is completely different compared to the fast propagating fractures during extension (Animation 1). Under compression stress concentration at the tips of the small mode I fractures are not high enough to support propagation. They cannot release compressive stress within the layer; they can only accommodate extension perpendicular to the shortening direction when the layer bulges.

Figure 2. Weaker matrix and layer parallel compression

Stiff vertical layer embedded in a weaker matrix and layer parallel compression. Colours show differential stress where red is high and blue low stress. Mode I fractures grow first, cluster into shear bands and lead to a transition where large scale shear fractures or faults cross the layer and induce failure. See main text for further explanation.

Figure 9. Transition between mode I and mode II fractures

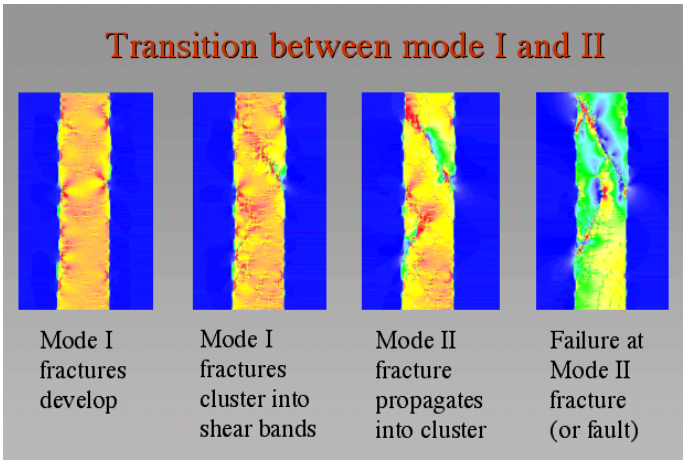

Transition between mode I and mode II fractures in a stiff layer under layer parallel compression. Stresses concentrate at geometrical irregularities on the interface of the stiff layer. Mode I fractures form in bands of compressive stresses and cluster in these bands. Later mode II type shear fractures develop out of the mode I clusters and form large-scale shear faults across the stiff layer. See main text for further explanation.

During progressive shortening of the layer regions of high stress concentrations from each side of the layer merge and form conjugate bands of high stress across the layer with an orientation of about 45° to the shortening direction. Small mode I fractures successively cluster in these bands. Finally shear or mode II fractures start to develop along the small mode I fractures within bands of high stress and propagate across the layer with an angle of less than 45° to the shortening direction. The shear fracture at the top of the

layer forms a through-cutting fracture or fault along which slip takes place. The second shear fracture that develops at the lower left of the competent layer propagates towards this fault but does not merge with it and instead curves to become parallel with the fault. Both shear fractures or faults are repelling each other, which results in a distinct spacing. Close to the interface of the competent layer to the matrix sets of conjugate shears develop along the faults. Strain is mostly localized in the upper fault where significant slip takes place so that even the incompetent surrounding matrix is fractured at the fault tip.

The development of small mode I fractures, clustering of mode I fractures into bands and transition to mode II shear fractures can be theoretically predicted [Toussaint and Pride 2002] and is found in similar models [Hazzard et al. 2000] and real rock experiments [Lockner et al. 1991]. Mode II shear fractures in the second simulation (animation 2) have a different spacing than the mode I fractures in the first simulation (animation 1). Spacing of mode II fractures is narrower and seems to be influenced by the spacing of initial irregularities on the interface, which is connected to the initial grain size in the model. Mode II fractures split grains in contrast to mode I fractures that tend to develop along grain boundaries. Mode II fractures are more straight than mode I fractures since they are not opening but accommodate slip which is less efficient if they are not straight.

Fracturing of polycrystalline material with a statistical distribution of grains

Two simulations were performed to investigate the development of fracture patterns in polycrystalline aggregates under pure shear deformation. The initial microstructure of the aggregates and the resolution of the models differ. The first simulation has the same initial microstructure as Animation 1 and 2 (Figure 5a), whereas the second simulation has a microstructure with smaller grains (Figure 5b). The resolution of the first simulation is 184800 particles (400x462) and the second simulation has a resolution of 737600 particles (800x922). Both simulations have distributed elastic constants for different grains and a distribution of tensile strengths of springs. The elastic constants of grains are distributed randomly and follow a Gauss distribution with a given mean m and the standard variation s. The resulting polycrystalline aggregate has a mean elastic constant of m. The tensile strength of springs is dispersed using a linear distribution with a given minimum and maximum value. Spring constants are chosen randomly within this distribution for all springs. Changing the width of the spring distribution changes the material behavior. Although the mean breaking strength will not change, the weakest springs act in a similar way to microflaws in the Griffith model [Griffith 1920] and concentrate stresses once they break. On a macroscopic scale this will result in a weaker strength of the material if the distribution is larger. Another effect is that material with a wider distribution of breaking strengths of springs will behave less brittle than a material with a very narrow range of breaking strengths. Once the tensile strength is reached in an aggregate with a narrow distribution failure will take place almost simultaneously throughout the whole deformation box. A wide distribution will produce initially a localization of failure at a restricted number of springs, which results in a more "ductile" behavior of the material on large scale.

The lower resolution simulation is shown in Animation 3 and Animation 4 , animation 3 illustrates the fracture pattern and animation 4 the differential stress. The higher resolution simulation is shown in Animation 5 where the fracture pattern is highlighted in order to compare it with animation 3. Both simulations are performed with pure shear boundary conditions where compression is vertical and extension horizontal. The Gauss distribution for elastic constants of grains is the same for both simulations with a mean elastic constant m of 2.0 and a standard variation s of + - 0.3. The distribution of the breaking strength of springs is different for both simulations; the distribution is narrower in the first simulation and wider in the second simulation (0.0048-0.0072 and 0.0036-0.0084). The models are deformed with a stepped compressive strain of 0.06 percent and the area of the deformation box is kept constant. Colors in animation 3 and 4 show the pressure, which is the sum of the normal stress in the vertical and horizontal direction. Particles that have broken springs appear in blue.

Figure 3. Polycrystalline rock

Polycrystalline rock with a statistical distribution of grains under pure shear deformation. Colours indicate the pressure and particles with fractured springs are blue. At first mode I fractures develop and are followed by mode II shear fractures. Both show a distinct spacing. See main text for further explanation.

Figure 4. Development of the differential stress

The same simulation as animation 3 showing development of the differential stress. See main text for further explanation.

Figure 5. Large resolution simulation

Large resolution simulation similar to animation 3 but with a wider distribution in breaking strengths of springs. The evolution of structures is similar in animation 3 and 5 but animation 5 shows more dispersed development of fractures due to the wider distribution in breaking strengths.

At first the distribution of elastic constants for different grains can be seen when grains show different stress-colors. Initial fractures start to develop around grains with higher elastic constants where tensile stresses are highest. They soon start to form larger scale mode I fractures that are oriented roughly parallel to the compressive stress. Mode I fractures develop first since the tensile strength of the aggregate is less than its compressive strength. The fractures reduce the tensile stress in the horizontal direction. Three large fractures develop initially with a distinct spacing. The polycrystalline material in animation 3 has a narrower distribution of breaking thresholds than that of animation 5, so that it behaves more brittle. Animation 5 shows a material with a wider distribution of breaking thresholds and consequently behaves more ductile, fractures are more dispersed, cluster in pairs and show a spacing that is not as distinct as the spacing in animation 3.

Mode I fractures in both simulations cannot relax the compressive stress. Therefore shear fractures develop shortly after the development of the extensional fractures. These shear fractures form conjugate sets with an angle of about 35° to the compressive stress. They are propagating relatively straight in animation 3 where they cross most grains. They also tend to cross mode I fractures but sometimes merge into them. They are often repelled at the boundaries of the model. A characteristic spacing seems to exist but it is not as clear as the spacing of mode I fractures. If slip takes place along mode II fractures new small conjugate sets of shear fractures develop along the original fracture due to friction. Slip along shear fractures is the main mechanism to reduce compressive vertical stresses. Animation 5 shows a more continuous transition from mode I fracturing through hybrid shears or coupled extension and shear fracturing to pure mode II fractures. Conjugate sets of shear fractures develop at the same angle of 35° to the compression as in animation 3. The shear-fracture pattern of animation 5 is different to that of animation 3 because of a wider distribution of breaking thresholds of springs in animation 5. This produces a more dispersed localization of fractures so that these are more irregular and not as straight as the shear fractures in animation 3. However, one has to note that the finite strain in animation 5 is lower than that of animation 3 so that in animation 5 significant slip along shear fractures has not yet taken place.

Animation 4 shows the differential stress in the low-resolution simulation. The stress scale is the same as the one in the previous chapter where red represents high differential stresses and blue low differential stresses. The initial stress distribution reflects the distribution of elastic properties of grains. Once mode I fractures develop they cause stress concentrations at their advancing tips (yellow to red) and they relax stresses while they grow (blue). Once shear fractures develop they separate regions of high stress (yellow to red) from regions of low stresses (blue). In order to reduce the compressive stress significantly slip takes place along shear planes. The initial mode I fractures plus shear fractures produce columns that support the vertical load. At the end of animation 5 the column in the middle of the deformation box fails through a large scale shear fracture and the stress within the whole column is suddenly released (becomes blue). This failure is similar to the one that took place in animation 2 where a vertical competent layer was shortened. The differential stress in the whole deformation box increases upon loading, it drops shortly once mode I fractures run through the whole box, increases again and drops significantly once mode II fracturing produces failure of load supporting columns. The development and size of these columns is influenced by the initial spacing of mode I and mode II fractures.

Expansion of single grains

Temperature and stress changes as well as the addition of fluid to a natural system may induce the growth of new minerals, which may include an increase in volume. This will lead to fractures in the surrounding matrix, which will enhance the permeability of a rock and influence its rheology. In this paragraph we show an example of fracture patterns that develop around several expanding grains. Animation 6 shows the fracture network and the pressure and Animation 7 the differential stress. The grains are forced to expand by increasing the radius of the intragrain particles by 0.01 percent per time step. A linear distribution

is used to disperse the breaking threshold of springs and grain boundaries are weaker as described above. No deformation is applied at the boundaries of the deformation box, instead the area of the box remains constant (walls are fixed).

Figure 6. Expansion of grains

Expansion of grains that produces branching crack patterns. Animation shows fracture pattern (blue colour) and the pressure.

Figure 7. Colour scale showing the differential stress

Same as animation 6 but with a colour scale showing the differential stress. See main text for further explanation.

The fracture network that develops (Animation 6) shows no preferred orientation because no external anisotropic stress is applied. Fractures form around the expanding grains and grow in a number of directions into the matrix. They branch once they have reached a characteristic distance from the expanding grain. Fractures tend to follow grain boundaries due to lower breaking thresholds but may also cross grains. In addition to the fractures that grow from the expanding grain into the matrix grain boundaries may also fail in front of the main fracture.

The differential stress in animation 7 is highest around the expanding grains. The stress initially forms rings around the expanding grains with the highest stress at the contact between the grain and the matrix. This geometry changes once fractures develop into the surrounding matrix. Fractures separate regions of high stress values from regions of low stress values. This suggests that they are shear fractures where compressed grains (regions of high stress) slide against regions of low stress. Each time the differential stress reaches a certain value next to the expanding grain (red colour) a new set of fractures develops or fractures propagate further into the matrix in order to relax stresses again. Load supporting grains between neighbouring expanding grains start to form stress bridges.

Discussion

The presented model offers the possibility to study fracture dynamics of rocks with varying initial microstructures. The model reproduces realistic behaviour of brittle materials. It is able to reproduce transitions between different types of fractures, shows realistic differences between materials under extension versus compression and produces realistic fracture patterns with a distinct spacing and geometry. Similar transitions from Mode I small-scale fractures toward large scale shear faults were found in experiments [Lockner et al. 1992], theoretical models [Toussaint and Pride 2002] and similar numerical approaches [Hazzard et al. 2000]. Hazzard et al. (2000) present a failure study mimicking compression tests with a commercial discrete element code (PFC). They compare their results with real rock experiments and conclude that this type of micromechanical model can reproduce real rock experiments including the full dynamics of crack propagation. The models also reproduce realistic stress-strain relationships. The different macroscopic behaviour of material in our simulations with varying distributions for fracture strength is similar to the results of Mogi (1962) who realized that the fracture process strongly depends on the degree of heterogeneity of materials. The material with narrow distributions of breaking strength in our simulations is more homogeneous and fails more suddenly whereas the material with a wide distribution behaves more ductile and shows small scale crack growth preceding failure. These differences are fundamental for earthquake prediction [Mogi 1962] and can be modelled with the presented approach. In addition this discrete type of model was found to reproduce the visual and statistical properties of fracture patterns from clay extension experiments [Malthe-Sørenssen et al. 1998]. The fracture patterns seen in animation 6 are similar to discharge patterns found during dielectric breakdown [Niemeyer et al. 1984] and colloidal aggregation, which have statistical similarities to natural fracture patterns [Meakin 1988].

The presented model can be used to simulate brittle failure in polycrystalline aggregates as shown. It is however also possible to combine the model with dissolution kinetics [Koehn et al. this volume], fluid pressure to model hydro fractures [Flekkøy et al. 2002], to use random lattices in order to avoid anisotropies of facture networks, to include visco-elastic behaviour and to evolve to a three-dimensional geometry. The model can have a very high resolution (Animation 5) in order to avoid effects of the discreteness of particles. Models up to two million particles are possible without using parallel coding since computer power has increased significantly over the last years. The model is not limited to any scale so that orogenic processes or metre scale faulting may be modelled as well as structures on a small scale as shown here.

A problem of the presented model is the triangular geometry of the network. It has the advantage that it reproduces linear elasticity on a large scale. However, it has the disadvantage that fracture propagation is not necessarily isotropic. Especially shear fractures along which slip takes place may develop along lattice directions. One possibility to suppress lattice directions is to define on the one hand a network of grains where grain boundaries break easier and on the other hand a distribution of spring strengths that is isotropic. This combination can help to avoid anisotropies of fracture networks due to the geometry of the underlying lattice. The distributions of breaking strengths work rather well with mode I fractures that show no preferred lattice orientation but is problematic for shear fractures. However, even shear fractures curve in the models (Animation 2) and change their propagation direction suggesting that the anisotropy of the underlying lattice is not that important. The same applies for the branching structures in animation 6 where a number of different orientations exist that are not triangular. However, small-scale anisotropies may still exist even with large distributions of spring breaking strengths.

Conclusion

A combination of a discrete particle code with elastic particle interactions and the possibility to fracture was coupled with the numerical model "Elle" in order to study fracture development in complex layered and polycrystalline materials. A number of simulations have been carried out to test the behaviour of fractures in the model and the developing patterns. The model produces realistic behaviour and spacing of mode I fractures during layer parallel extension and a theoretically predicted transition from mode I to mode II fractures during layer parallel compression. The behaviour of the model during pure shear deformation is also realistic and shows an expected initial development of mode I fractures due to low tensile strength of the material and a later propagation of shear fractures along which slip takes place. Fracture patterns around expanding grains produce isotropic patterns that are similar to dielectric breakdown that has similarities to natural fracture patterns. We conclude therefore that the model can be used to simulate brittle behaviour of materials and has a large applicability in future research.

Acknowledgements

Part of this research was funded by a grant from the Center of Advanced Studies of the Norwegian Academy of Sciences and by the EU-Network "Precip-Dissolution" contract number HPRN-CT-2000-00058. JA acknowledges funding by the DFG-Graduiertenkolleg "Composition and Evolution of Crust and Mantle". We thank Anders Malthe-Sørenssen for all his help with the discrete particle code, Mark Jessell, Lynn Evans and Paul Bons for their help with "Elle" and Rianne Brunt, Renault Toussaint, Cees Passchier and Bjørn Jamtveit for helpful discussions.

References

Allen, D.M.d.G. 1954. Relaxation methods, McGraw Hill, New-York, 257 pp.

Bons, P.D., Jessell, M.W., Evans, L., Barr, T.D., Stüwe, K., 2000. Modelling of anisotropic grain growth in minerals. In: Tectonic Modeling: a Volume in Honor of Hans Ramber, Memoir 193 (eds. Koyi, H.A., Mancktelow, N.S.), Geological Society of America, Boulder, Co. 45-49.

D'Ardetta, G.A., Kun, F., Ramm, E., Herrmann, H.J., 2001. From solids to granulates – Discrete element simulations of fracture and fragmentation processes in geomaterials. In "Continuous and Discontinuous Modelling of Cohesive-Frictional Materials", ed. Vermeer, P.A., Diebels, S., Ehlers, W., Herrmann, H.J., Luding, S., Ramm, E., Lecture Note in Physics, Vol. 568, 231-258.

Flekkoy, E.G., Malthe Sorensen, A. and Jamtveit, B. 2002. Modeling hydro-fracture. Journal of Geophysical Research, B8.

Griffith, A.A., 1920. The phenomena of rupture and flow in solids. Trans. Roy. Soc. Phil. Ser. A, 221, 163-198.

Hazzard, J.F., Young, R.P. and Maxwell, S.C., 2000. Micromechanical modeling of cracking and failure in brittle rocks. J. Geophys, Res. 105, 16,683-16,698.

Jaeger, J. and N.G.W. Cook, 1979. Fundamental of Rock Mechanics, Chapman & Hall, London, 3rd edition, 593 pp.

Jessell, M. W., Bons, P.D., Evans, L., Barr, T., Stuewe, K., 2001. Elle: the numerical simulation of metamorphic and deformation microstructures, Computers And Geosciences 27, 17-30.

Jessell, M. W., Kostenko, O. and Jamtveit, B., 2003. The preservation potential of microstructures during static grain growth. Journal of Metamorphic Geology, 21, 481-491.

Lockner, D.A., Byerlee, J.D., Kuksenko, V., Ponomarev, A., Sidorin, A., 1991. Quasi-static fault growth and shar fracture energy in granite, Nature, 350(7), 39-42.

Lockner, D.A. 1998. A generalized law for brittle deformation of Westerly granite. J. Geophys. Res. 103, 5107-5123.

Malthe-Sørenssen, A., Walmann, T., Feder, J., Jossang, T. and Meakin, P. 1998. Simulation of extensional clay fractures. Physical Review E., 58(5) , 5548-5564.

Marder, M., 1993. Cracks take a new turn. Nature, 362, p. 295.

Meakin, P. 1988. Simple models for colloidal aggregation, dielectric breakdown and mechanical breakdown patterns. In "Random Fluctuations and Pattern Growth", ed. H.E. Stanley and N. Ostrowsky. Kluwer, Dordrecht.

Means, W.D., 1976. Stress and Strain: basic concepts of continuum mechanics for Geologists. Springer-Verlag, New York, 339pp.

Mogi, K., 1962. Study of elastic shocks caused by the fracture of heterogenous materials and their relation to earthquake phenomena. Bull. Earthquake Res. Inst. Univ. Tokyo 40: 125-173.

Mühlhaus, H.-B., Sakaguchi, H., Moresi, L., Fahey, M. 2001. Discrete and continuum modelling of granular materials. In "Continuous and Discontinuous Modelling of Cohesive-Frictional Materials", ed. Vermeer, P.A., Diebels, S., Ehlers, W., Herrmann, H.J., Luding, S., Ramm, E., Lecture Note in Physics, Vol. 568, 185-204.

Niemeyer, L., Pietronero, L. and Wiesmann, H.J. 1984. Fractal dimension of dielectrical breakdown. Physical Review Letters, 52 , 1033.

Okui, Y. and Horii, H., 1997. Stress and time-dependent failure of brittle rocks under compression: A theoretical prediction. J. Geophys. Res. 102(B7), 14869-14881.

Paterson , M.S., 1978. Experimental Rock deformation – brittle field. Berlin: Springer Verlag.

Piazolo, S., Jessell, M.W., Bons, P.D., Evans, L., 2001. Animations of dynamic recrystallization with the numerical modelling system Elle. Journal of the Virtual Explorer 4. http://virtualexplorer.com.au/2001/Volume4/.

Piazolo, S., Bons, P.D., Jessell, M.W., Evans, L., Passchier, C.W., 2002. Dominance of Microstructural Processes and their effect on microstructural development: Insights from Numerical Modelling of dynamic recrystallisation. In: Deformation Mechanisms, Rheology and Tectonics: Current Status and Future Perspectives, Spcial Publication, 200 (eds. De Meer, S., Drury, M.D., De Bresser, J.H.P., Pennock, G.M.), Geological Society, London, 149-170.

Pollard, D.D. and Segall, P. 1987. Theoretical displacements and stresses near fractures in rocks: with applications to faults, joints, dikes and solution surfaces. In: Fracture mechanics of Rock. Ed. B.K. Atkinson. London: Academic press, 277-.348.

Price, N.J. and Cosgrove, J.W., 1990. Analysis of geological structures. Cambridge: Cambridge University Press.

Ranalli, G. 1995. Rheology of the earth. Second edition. Kluwer Academic Publishers, Dordrecht, 432 pp.

Scholz, C.H. 2002. The mechanics of Earthquakes and faulting, 2nd edition, Cambridge: Cambridge Univ. Press.

Shaw, F.S., 1953. An introduction to relaxation methods, New York Dover Publications, 396 pp.

Toussaint, R. and Pride, S.R. 2002. Fracture of disordered solids in compression as a critical phenomenon: I. Statistical mechanics formalism. Phys. Rev. E 66, art. 036135.